



## Invited

# Degenerate Bogdanov–Takens bifurcations in a one-dimensional transport model of a fusion plasma



H.J. de Blank<sup>a</sup>, Yu.A. Kuznetsov<sup>b</sup>, M.J. Pekkér<sup>c,1</sup>, D.W.M. Veldman<sup>b,\*</sup>

<sup>a</sup> FOM Institute DIFFER - Dutch Institute for Fundamental Energy Research, The Netherlands

<sup>b</sup> Mathematisch Instituut, Utrecht University, Budapestlaan 6, 3584CD Utrecht, The Netherlands

<sup>c</sup> Mathematical Sciences Department, University of Alabama in Huntsville, Huntsville, AL 35899, United States

## HIGHLIGHTS

- A new method for continuation of Bogdanov–Takens bifurcations in large ODE systems.
- The dynamics of a fusion plasma model is studied by numerical continuation.
- A (codimension-2) Bogdanov–Takens bifurcation is continued in three parameters.
- Along the curve, a codimension-4 degenerate Bogdanov–Takens bifurcation is detected.
- This nongeneric event is robust under changes in the additional parameters.

## ARTICLE INFO

### Article history:

Received 4 February 2016

Accepted 17 May 2016

Available online 24 May 2016

Communicated by B. Sandstede

### Keywords:

L–H transition

Bifurcations theory

Numerical continuation

Large-scale systems

MATLAB

## ABSTRACT

Experiments in tokamaks (nuclear fusion reactors) have shown two modes of operation: L-mode and H-mode. Transitions between these two modes have been observed in three types: sharp, smooth and oscillatory. The same modes of operation and transitions between them have been observed in simplified transport models of the fusion plasma in one spatial dimension. We study the dynamics in such a one-dimensional transport model by numerical continuation techniques. To this end the MATLAB package CL\_MATCONTL was extended with the continuation of (codimension-2) Bogdanov–Takens bifurcations in three parameters using subspace reduction techniques. During the continuation of (codimension-2) Bogdanov–Takens bifurcations in 3 parameters, generically degenerate Bogdanov–Takens bifurcations of codimension-3 are detected. However, when these techniques are applied to the transport model, we detect a degenerate Bogdanov–Takens bifurcation of codimension 4. The nearby 1- and 2-parameter slices are in agreement with the presence of this codimension-4 degenerate Bogdanov–Takens bifurcation, and all three types of L–H transitions can be recognized in these slices. The same codimension-4 situation is observed under variation of the additional parameters in the model, and under some modifications of the model.

© 2016 Elsevier B.V. All rights reserved.

## 1. Introduction

In a tokamak fusion reactor, the plasma is confined in a solid torus by a magnetic field. Particles and energy are transported from the hot core to the cold edge of the torus. The performance of a

fusion reactor is largely determined by its energy confinement. Experiments have shown a ‘Low confinement mode’ (or L-mode) and a ‘High confinement mode’ (or H-mode) [1]. In H-mode, a transport barrier is formed near the edge. In L-mode this transport barrier is absent. This makes the energy confinement in H-mode typically twice as high as in L-mode. Transitions from L-mode to H-mode (and back) under change of heating have been observed in three types: sharp, smooth and oscillatory.

In order to understand the physical mechanisms relevant to these transitions, the dynamics of the tokamak plasma has been studied in one-dimensional transport models. One of the first of these models that showed all three types of L–H transitions was proposed by Itoh et al. [2]. The extension of this model by

\* Corresponding author.

E-mail addresses: [h.j.deblank@diffier.nl](mailto:h.j.deblank@diffier.nl) (H.J. de Blank), [i.a.kouznetsov@uu.nl](mailto:i.a.kouznetsov@uu.nl) (Yu.A. Kuznetsov), [mark.pekker@uah.edu](mailto:mark.pekker@uah.edu) (M.J. Pekkér), [d.w.m.veldman@tue.nl](mailto:d.w.m.veldman@tue.nl) (D.W.M. Veldman).

URL: <http://www.diffier.nl> (H.J. de Blank).

<sup>1</sup> Formerly M.J. Friedman.

Zohm [3] formed the basis of the series of papers by Weymiens et al. [4–6]. In these papers, bifurcation theory is used to study the arrangement of the different types of transitions in the parameter space. It was observed that all three types of L–H transitions could be explained by the presence of a degenerate Bogdanov–Takens (dBT) bifurcation [4]. This observation was supported by the two-dimensional bifurcation diagram resulting from an analytic approximation [5] and by parameter scans in a spatial discretization of the model [6]. However, the dBT bifurcation itself was not detected, neither in the analytic approximation nor in the spatial discretization.

The considered transport models consist of nonlinear evolution PDEs on a one-dimensional spatial domain. The solutions of these PDEs are typically studied by considering their spatial discretization, which typically results in large systems of ODEs with large and sparse Jacobian matrices. Information about bifurcations of equilibria is typically contained in a small invariant subspace, corresponding to rightmost eigenvalues of the Jacobian matrix [7]. In the MATLAB package `CL_MATCONT` [8], this subspace is computed efficiently using the Continuation of Invariant Subspaces (CIS) algorithm [9]. This makes `CL_MATCONT` suitable to study bifurcations of equilibria in large-scale systems. The code of `CL_MATCONT` is based on `CL_MATCONT` [10]. `CL_MATCONT` and its GUI version `MATCONT` [11,12] are MATLAB packages for study of bifurcations in small and moderate-size systems.

In this paper, `CL_MATCONT` and `MATCONT` are used to study the bifurcations in the one-dimensional transport model studied by Weymiens et al. [4–6]. Numerical continuation techniques and normal form computations have not been applied to this model before. These techniques result in higher resolution bifurcation diagrams than have been obtained in [6] and enable the detection of dBT bifurcations. To this end, the continuation of Bogdanov–Takens (BT) bifurcations in 3-parameters using subspace reduction techniques has been added to `CL_MATCONT`. During the 3-parameter continuation of the BT bifurcation in the transport model, a codimension-4 degenerate BT bifurcation is found. This event is nongeneric in a 3-parameter continuation. We have verified that this event is not caused by a nongeneric choice of the additional parameter in the model, and that this codimension-4 situation remains present under natural modifications of the model. Other novel features in this paper are an analytic approximation of equilibrium solutions of the one-dimensional transport model, which is used to find a starting point for the continuation, and an efficient spatial discretization for this model.

The rest of the paper is organized as follows. In Section 2, we provide the theoretical background. In particular, in Section 2.1 the bifurcation theory of the dBT bifurcations of codimension 3 and 4 relevant for this paper is reviewed, and in Section 2.2 the continuation BT bifurcations using subspace reduction techniques is discussed. In Section 3, the one-dimensional transport model is introduced, (analytic approximations for) its equilibrium solutions are discussed, and a spatial discretization is presented. In Section 4, the bifurcations in this spatial discretization are studied using `CL_MATCONT` and `CL_MATCONT`. Section 5 contains a discussion of the results. Appendix discusses new features of the code of `CL_MATCONT` compared to the description of its first version in [7].

## 2. Theoretical background

### 2.1. Degenerate Bogdanov–Takens bifurcations

We consider a system of ODEs,

$$\dot{u} = f(u, \alpha), \quad u \in \mathbb{R}^n, \alpha \in \mathbb{R}^p, \quad (1)$$

which is typically the result of a spatial discretization of a (system of) PDEs and introduce the Jacobian matrix  $A := f_u(u, \alpha) \in \mathbb{R}^{n \times n}$ .

**Table 1**

Relevant codimension-1 bifurcations.

LP	Limit Point or fold or saddle-node
H	Hopf
HHS	Homoclinic to Hyperbolic Saddle
HSN	Homoclinic to Saddle-Node

**Table 2**

Relevant codimension-2 bifurcations.

CP	Cusp
GH	Generalized Hopf or Bautin
BT	Bogdanov–Takens
NSH	Neutral Saddle Homoclinic
NCH	Non-Central Homoclinic

In this section, we discuss the bifurcations in the setting of ODEs. However, it should be noted that these bifurcations also occur in PDEs. We assume the reader is familiar with standard bifurcation theory, in particular with the bifurcations of codimension 1 and 2 listed in Tables 1 and 2 (see e.g. [13]).

At a BT bifurcation, the Jacobian matrix  $A$  at an equilibrium has a double zero eigenvalue of geometric multiplicity one and no other critical eigenvalues. In other words, the Jordan block associated with this eigenvalue is of the form

$$\begin{bmatrix} 0 & 1 \\ 0 & 0 \end{bmatrix}.$$

At the critical parameter values there exists a smooth coordinate change which brings the restriction to the center manifold to the form (see [14])

$$\begin{cases} \dot{y}_1 = y_2, \\ \dot{y}_2 = \sum_{k \geq 2} a_k y_1^k + b_k y_1^{k-1} y_2^k. \end{cases} \quad (2)$$

The bifurcation scenario near the BT bifurcation is determined by the normal form coefficients  $a_k$  and  $b_k$ .

In the generic (codimension-2) situation the normal form coefficients  $a_2$  and  $b_2$  are both nonzero. The situation near this BT bifurcation is characterized by the 2-parameter universal unfolding (see, e.g. [14,13])

$$\begin{cases} \dot{y}_1 = y_2, \\ \dot{y}_2 = \beta_1 + \beta_2 y_2 + a_2 y_1^2 + b_2 y_1 y_2. \end{cases} \quad (3)$$

For this situation, the complete bifurcation diagram is available and includes LP, H and HHS bifurcations.

Possible degeneracies involve the vanishing of the normal form coefficients  $a_2$  and  $b_2$ . Codimension-3 situations occur when only one of these coefficients vanishes. A codimension-4 situation occurs when both coefficients vanish simultaneously.

For the (codimension-3) case, where  $b_2 = 0$  and  $a_2 \neq 0$ , a three parameter universal unfolding is (see [15])

$$\begin{cases} \dot{y}_1 = y_2, \\ \dot{y}_2 = \beta_1 + \beta_2 y_2 + \beta_3 y_1 y_2 + a_2 y_1^2 + b_4 y_1^3 y_2. \end{cases} \quad (4)$$

This bifurcation is also called a *dBT with a double equilibrium*. This system has been studied by Dumortier et al. [16]. Fig. 1 shows the bifurcation diagram for this situation, which has been obtained under the transformation

$$(\beta_1, \beta_2, \beta_3) = (r \sin(\theta), \beta_2, r \cos(\theta)),$$

with  $r = 0.1$ . Similar bifurcation diagrams can be obtained for smaller values of  $r$ , since the 3D bifurcation diagram of (4) in the  $\beta$ -space has a conic structure near the origin. This is also true for other canonical unfoldings appearing below.

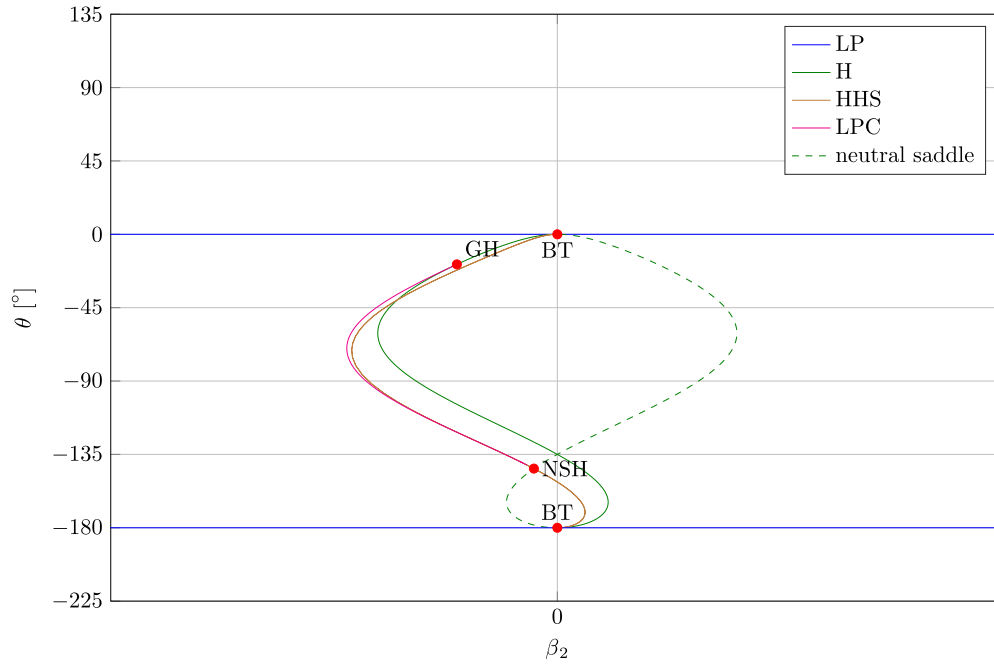


Fig. 1. Bifurcation diagram of the unfolding (4) for  $a_2 = b_4 = 1$  (with  $r = 0.1$ ).

The other codimension-3 case, where  $a_2 = 0$  and  $b_2 \neq 0$ , can be unfolded as (see [15])

$$\begin{cases} \dot{y}_1 = y_2, \\ \dot{y}_2 = \beta_1 + \beta_2 y_1 + \beta_3 y_2 + a_3 y_1^3 + b_2 y_1 y_2 + b'_3 y_1^2 y_2, \end{cases} \quad (5)$$

where

$$b'_3 = b_3 - \frac{3b_2}{5a_3}.$$

This bifurcation is also called a *dBt with a triple equilibrium*. Depending on the values of  $a_3$  and  $b_2$ , there are three subcases, which have been studied in great detail by Dumortier et al. [17], although some gaps prevent calling (5) the universal unfolding. Fig. 2 shows the bifurcation diagram for the so called *focus* subcase where  $a_3 < 0$  and  $b_2^2 + 8a_3 < 0$ , which is obtained under the transformation

$$(\beta_1, \beta_2, \beta_3) = (\beta_1, r \cos(\theta), r \sin(\theta)),$$

with  $r = 0.1$ .

The codimension-4 situation when  $a_2 = b_2 = 0$  is most relevant for this paper. A 4-parameter universal unfolding of this singularity is conjectured to be (see [18])

$$\begin{cases} \dot{y}_1 = y_2, \\ \dot{y}_2 = \beta_1 + \beta_2 y_1 + \beta_3 y_2 + \beta_4 y_1 y_2 + a_3 y_1^3 + b_3 y_1^2 y_2. \end{cases} \quad (6)$$

There are two subcases depending on the value of  $a_3$ . The subcase  $a_3 > 0$  has (to our best knowledge) not been studied in literature. The physically most relevant subcase for  $a_3 < 0$  has been studied by Khibnik et al. [18]. For this subcase, the bifurcation diagram for  $\beta_4 = 0$  is shown in Fig. 3, which has been obtained under the transformation

$$(\beta_1, \beta_2, \beta_3, \beta_4) = (\beta_1, r \cos(\theta), r \sin(\theta), \beta_4),$$

with  $r = 0.001$ . At the points labeled 'NCH (2x)', there are two NCH bifurcations connected by a curve of HSN bifurcations (the same situation is visible in Fig. 2). Note that (6) is invariant under the transformation

$$(y_1, y_2, \beta_1, \beta_2, \beta_3, \beta_4) \mapsto (-y_1, -y_2, -\beta_1, +\beta_2, +\beta_3, -\beta_4),$$

which explains the symmetry around  $\beta_1 = 0$  in Fig. 3. When  $\beta_4 \neq 0$  this symmetry is destroyed and other bifurcation diagrams may appear, see [18] for a more detailed discussion.

## 2.2. Continuation of BT bifurcations

The continuation methods for bifurcations using *minimally augmented systems* can be found in [19]. Minimally augmented systems provide an efficient way to detect singularities of a matrix  $A(s) \in \mathbb{R}^{n \times n}$ , depending on a parameter  $s$ . For example, to detect that an eigenvalue  $\lambda_i(s)$  of  $A(s)$  becomes zero, one might check whether  $\det(A(s)) = \prod \lambda_i(s)$  changes sign. However, the computation of the determinant is computationally demanding and even for moderate-size systems the values of  $\det(A(s))$  can become very large or small. Therefore, it is better to check whether another function  $g(s)$  changes sign (see [19,13]), where  $g(s)$  is the solution to the bordered system

$$\begin{bmatrix} A(s) & w_{\text{bor}} \\ v_{\text{bor}}^\top & 0 \end{bmatrix} \begin{bmatrix} v \\ g(s) \end{bmatrix} = \begin{bmatrix} 0_m \\ 1 \end{bmatrix}. \quad (7)$$

We use the following notation for zero matrices:  $0_{n \times m}$  will denote an  $(n \times m)$ -zero matrix,  $0_m$  denotes a  $m$ -dimensional column vector of zeros, and 0 will always denote a scalar zero. Clearly, the vectors  $v_{\text{bor}}, w_{\text{bor}}$  must be chosen such that the matrix on the left of (7) is nonsingular. In a continuation algorithm (see e.g. [7]), the border  $v_{\text{bor}}$  is typically set to solution  $v$  of (7) computed at the previous step and the border  $w_{\text{bor}}$  is set to  $w$ , where  $w$  is the solution of the transposed bordered system

$$\begin{bmatrix} A^\top(s) & v_{\text{bor}} \\ w_{\text{bor}}^\top & 0 \end{bmatrix} \begin{bmatrix} w \\ g(s) \end{bmatrix} = \begin{bmatrix} 0_m \\ 1 \end{bmatrix}, \quad (8)$$

also computed at the previous continuation step. Using the solutions of (7) and (8), one can also efficiently compute the derivative of  $g(s)$  w.r.t.  $s$  by

$$g_s(s) = -w^\top A_s(s) v. \quad (9)$$

To study the bifurcations of the system (1), we consider  $A(s) := f_u(u(s), \alpha(s))$  the Jacobian matrix along a curve  $(u(s), \alpha(s))$  of equilibria. For large-scale systems, typically only a few eigenvalues of  $A(s)$  are located near the imaginary axis and are relevant for bifurcation analysis. The CIS algorithm computes a smooth orthonormal basis  $Q(s)$  of the (right) eigenspace of  $A(s)$  corresponding to

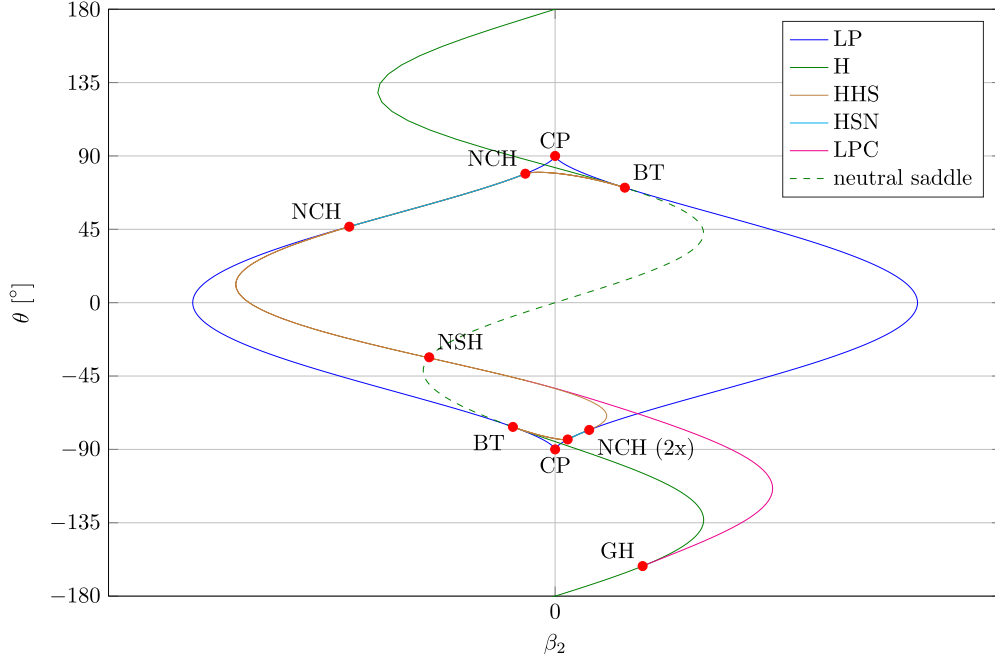


**Fig. 2.** Bifurcation diagram of the unfolding (5) for  $a_3 = -1$ ,  $b_2 = 1$  and  $b'_3 = 1$  (with  $r = 0.1$ ).

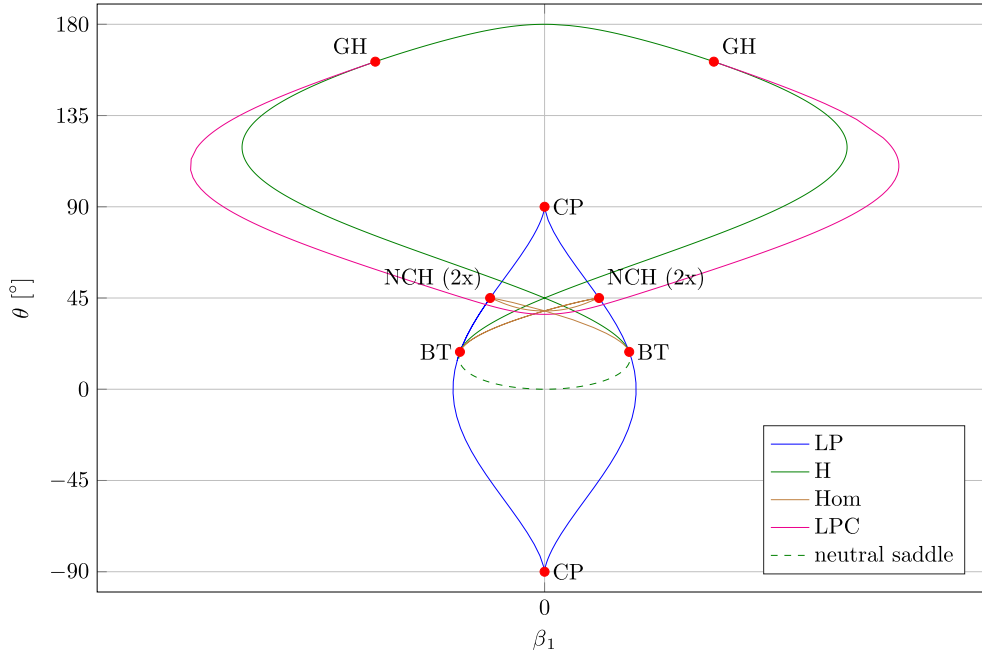


**Fig. 3.** Bifurcation diagram of the system (6) for  $a_3 = b_3 = -1$  for  $\beta_4 = 0$  (with  $r = 0.001$ ).

the  $m \ll n$  right most eigenvalues of  $A(s)$ . The restriction of  $A(s)$  to the subspace  $Q(s)$  is denoted by

$$C(s) := Q(s)^\top A(s) Q(s). \quad (10)$$

By construction, the  $m$  rightmost eigenvalues of  $A(s)$  are the eigenvalues of  $C(s)$ . Therefore, bifurcations can be detected efficiently by considering the much smaller matrix  $C(s)$ .

The minimally augmented system for the BT-curve can be found in [19]. Here we combine this approach with subspace reduction techniques. The defining system for the Bogdanov–Takens curve is now  $F(X) = 0$ , where

$$X = (u, \alpha) \in \mathbb{R}^n \times \mathbb{R}^3, \quad F(X) = \begin{pmatrix} f(u, \alpha) \\ g_1(u, \alpha) \\ g_2(u, \alpha) \end{pmatrix}.$$

Here,  $f$  is as in (1) and  $g_1$  and  $g_2$  are now computed based on the restriction  $C$  as

$$\begin{bmatrix} C & \hat{w}_{\text{bor}} \\ \hat{v}_{\text{bor}}^\top & 0 \end{bmatrix} \begin{bmatrix} \hat{v}_1 \\ g_1 \end{bmatrix} = \begin{bmatrix} 0_m \\ 1 \end{bmatrix}, \quad (11)$$

$$\begin{bmatrix} C & \hat{w}_{\text{bor}} \\ \hat{v}_{\text{bor}}^\top & 0 \end{bmatrix} \begin{bmatrix} \hat{v}_2 \\ g_2 \end{bmatrix} = \begin{bmatrix} \hat{v}_1 \\ 0 \end{bmatrix}, \quad (12)$$

where the borders  $\hat{v}_{\text{bor}}, \hat{w}_{\text{bor}} \in \mathbb{R}^m$  must be selected such that the matrix on the LHS is nonsingular. In practice, this means that  $\hat{v}_{\text{bor}}$  is equal to the solution  $\hat{v}_1$  computed at the previous continuation step and  $\hat{w}_{\text{bor}}$  is computed from the solution to the transposed system of (11) at the previous continuation step (similar to (8)).

It now holds that (see [19])

$$g_1 = g_2 = 0 \quad \Leftrightarrow \quad p(0) = p_\lambda(0) = 0, \quad (13)$$

where  $p(\lambda) = \det(C - \lambda I)$  is the characteristic polynomial of  $C$ . So when  $g_1 = g_2 = 0$ ,  $p(\lambda)$  has a double zero, so  $C$  has a zero eigenvalue of multiplicity 2. This means that when  $F(X) = 0$ , we have an equilibrium ( $f = 0$ ) with an eigenvalue zero with multiplicity 2 ( $g_1 = g_2 = 0$ ), i.e. a BT bifurcation.

The curve of BT bifurcations  $X(s)$  is computed using *pseudo-arclength continuation* [20], for which the Jacobian matrix  $F_X$  is needed. For the considered curve,

$$F_X = \begin{bmatrix} A & f_\alpha \\ g_{1,\alpha} & g_{1,\alpha} \\ g_{2,\alpha} & g_{2,\alpha} \end{bmatrix}. \quad (14)$$

The main novelty of our approach is the computation of the derivatives of  $g_1$  and  $g_2$ , which is based on the following lemma (cf. (9)).

**Lemma 1.** Let  $A = A(X) \in \mathbb{R}^{n \times n}$ ,  $Q = Q(X) \in \mathbb{R}^{n \times m}$ ,  $X \in \mathbb{R}^{n+p}$  and assume that the columns of  $Q$  span an invariant subspace of  $A$ . Also, let  $C = C(X)$  be as in (10). Further, assume that the borders  $\hat{v}_{\text{bor}}, \hat{w}_{\text{bor}} \in \mathbb{R}^m$  in (11) are chosen such that the matrix on the left of (11) is nonsingular and introduce  $\hat{v}_1, \hat{v}_2 \in \mathbb{R}^m$  and  $g_1, g_2 \in \mathbb{R}$  as solutions to (11) and (12). Now, define  $W_1, W_2 \in \mathbb{R}^n$  and  $\tilde{g}_1, \tilde{g}_2 \in \mathbb{R}$  as solutions of

$$\begin{bmatrix} A^\top & Q\hat{v}_{\text{bor}} \\ \hat{w}_{\text{bor}}^\top Q^\top & 0 \end{bmatrix} \begin{bmatrix} W_1 \\ \tilde{g}_1 \end{bmatrix} = \begin{bmatrix} 0_n \\ 1 \end{bmatrix}, \quad (15)$$

$$\begin{bmatrix} A^\top & Q\hat{v}_{\text{bor}} \\ \hat{w}_{\text{bor}}^\top Q^\top & 0 \end{bmatrix} \begin{bmatrix} W_2 \\ \tilde{g}_2 \end{bmatrix} = \begin{bmatrix} W_1 \\ 0 \end{bmatrix}. \quad (16)$$

Then the matrix on the left of (15) and (16) is nonsingular,  $g_1 = \tilde{g}_1$  and  $g_2 = \tilde{g}_2$ , and when  $g_1(X_0) = g_2(X_0) = 0$  it holds that

$$g_{1,X}(X_0) = -W_1^\top A_X Q_1 \hat{v}_1, \quad (17)$$

$$g_{2,X}(X_0) = -W_2^\top A_X Q_1 \hat{v}_1 - W_1^\top A_X Q_1 \hat{v}_2. \quad (18)$$

The proof can be found in the [Appendix A.4](#).

Because  $g_1$  and  $g_2$  are zero along the curve, the derivatives of  $g_1$  and  $g_2$  in (14) are computed as

$$g_{1,u} = -W_1^\top A_u Q \hat{v}_1, \quad g_{2,u} = -W_2^\top A_u Q \hat{v}_1 - W_1^\top A_u Q \hat{v}_2,$$

$$g_{1,\alpha} = -W_1^\top A_\alpha Q \hat{v}_1, \quad g_{2,\alpha} = -W_2^\top A_\alpha Q \hat{v}_1 - W_1^\top A_\alpha Q \hat{v}_2$$

where  $W_1$  and  $W_2$  are computed from (15) and (16).

At each found point  $X(s_k) = (u(s_k), \alpha(s_k))$ , the normal form coefficients  $a_2$  and  $b_2$  in the normal form (3) can be computed using the generalized eigenvectors of  $A$  satisfying

$$Aq_0 = 0_n, \quad Aq_1 = q_0, \quad A^\top p_1 = 0_n, \quad A^\top p_0 = p_1,$$

which are normalized such that  $p_0^\top q_0 = p_1^\top q_1 = 1$  and  $p_0^\top q_1 = p_1^\top q_0 = 0$ . The normal form coefficients  $a_2$  and  $b_2$  can then be computed as (see [13] or [15])

$$a_2 = \frac{1}{2} p_1^\top f_{uu}[q_0, q_0], \quad (19)$$

$$b_2 = p_0^\top f_{uu}[q_0, q_0] + p_1^\top f_{uu}[q_0, q_1], \quad (20)$$

where  $f_{uu}[r, s]$  is the second derivative of  $f$  w.r.t.  $u$  evaluated on the vectors  $r, s \in \mathbb{R}^n$ . The two codimension-3 degeneracies from Section 2.1 are now found when  $a_2$  or  $b_2$  changes sign along the computed curve. When such a degenerate situation is detected, the normal form coefficients  $a_3, b_3, a_4$  and  $b_4$  are computed using the formulas (similar to (19) and (20)) from [15].

The continuation of Bogdanov–Takens bifurcations in small and moderate-size systems was implemented in CONTENT [21], but is currently not supported by CL\_MATCONT or MATCONT.

### 3. Discretization of the transport model

#### 3.1. One-dimensional transport model

We use the same model as in [6]. This model describes the evolution of the particle density  $n$ , the temperature  $T$  and the radial electric field or poloidal rotation  $Z$  near the plasma edge and consists of the following system of nonlinear PDEs,

$$\frac{\partial n}{\partial t} = -\frac{\partial \Gamma}{\partial x}, \quad \Gamma = -D(Z) \frac{\partial n}{\partial x}, \quad (21)$$

$$\frac{\partial U}{\partial t} = -\frac{\partial q}{\partial x}, \quad q = -\chi(Z)n \frac{\partial T}{\partial x} + \frac{\Gamma T}{\gamma - 1}, \quad (22)$$

$$\varepsilon \frac{\partial Z}{\partial t} = \mu \frac{\partial^2 Z}{\partial x^2} + c_n \frac{T}{n^2} \frac{\partial n}{\partial x} + \frac{c_T}{n} \frac{\partial T}{\partial x} + G(Z), \quad (23)$$

where

$$D(Z) = D_0 + D_1 \tanh(Z), \quad (24)$$

$$\chi(Z) = \frac{1}{(\gamma - 1)\zeta} D(Z), \quad (25)$$

$$G(Z) = a - b(Z - Z_S) - (Z - Z_S)^3, \quad (26)$$

and the internal energy  $U$  is defined as

$$U = \frac{nT}{\gamma - 1}. \quad (27)$$

The spatial coordinate  $x$  represents radial coordinate in the (torus shaped) region occupied by the plasma. The (cold) plasma edge is located at  $x = 0$  and the (hot) plasma core is located at  $x = +\infty$ . Geometric effects originating from the curvature of the torus shaped surfaces have been neglected, because their effect near the plasma edge is small. Eq. (21) describes the transport of particles due to the particle flux  $\Gamma$ , which is related to the density gradient by a diffusivity  $D = D(Z)$ . Eq. (22) describes the transport of energy due to the heat flux  $q$ , which is driven by conduction and advection. Here  $\chi = \chi(Z)$  represents the (heat) conductivity of the plasma and  $\gamma$  is the adiabatic index and  $\zeta$  in (25) represents a proportionality factor. Eq. (23) describes the evaluation of the radial electric field or poloidal rotation. The first term represents the anomalous shear viscosity, the second and the third term are due to the bipolar part of anomalous cross field flux. The function  $G(Z)$  incorporates a variety of contributions to the radial current (see the appendix of [6] for a detailed discussion).

The boundary conditions at the edge of the plasma  $x = 0$  are

$$\frac{\partial n}{\partial x} = \frac{n}{\lambda_n}, \quad \frac{\partial T}{\partial x} = \frac{T}{\lambda_T}, \quad \frac{\partial^2 Z}{\partial x^2} = 0. \quad (28)$$

Here, the boundary conditions for  $n$  and  $T$  model a scrape-off layer at the edge of the plasma. The boundary conditions at the plasma core  $x = +\infty$  are

$$\Gamma = \Gamma_\infty, \quad q = q_\infty, \quad \frac{\partial Z}{\partial x} = 0. \quad (29)$$

The particle flux  $\Gamma_\infty$  takes into account the particles that are added to the plasma and the heat flux  $q_\infty$  describes the heat generated inside the plasma.

Unless stated otherwise, we will use the parameter values in Table 3. Note that we are only interested in the situation where particles and heat flow from the (hot) core to the (cold) edge, i.e. the case where  $\Gamma_\infty, q_\infty < 0$ .

#### 3.2. Equilibrium solutions

The equilibrium solutions are denoted  $\tilde{n}, \tilde{T}$  and  $\tilde{Z}$ . The equilibrium solutions  $\tilde{n}$  and  $\tilde{T}$  can be expressed in terms of the equilibrium



**Table 3**  
Standard parameter values.

Parameter	Value
$D_0$	1.9
$D_1$	−1.1
$\gamma$	5/3
$\zeta$	1.1
$\varepsilon$	0.05
$\mu$	0.05
$c_n$	1.1
$c_T$	0.9
$a$	−1
$b$	−1
$Z_S$	0
$\lambda_n$	1.25
$\lambda_T$	1.5
$\Gamma_\infty$	−0.8
$q_\infty$	−0.75
$L$	10

solution for the radial electric field  $\tilde{Z}$  as (see [4])

$$\tilde{n}(x) = n_0 - \Gamma_\infty \int_0^x \frac{dx'}{D(\tilde{Z}(x'))}, \quad (30)$$

$$\tilde{T}(x) = T_\infty + (T_0 - T_\infty) \left( \frac{n(x)}{n_0} \right)^{-\zeta}, \quad (31)$$

where  $Z_0 := \tilde{Z}(x=0)$ ,  $T_\infty = (\gamma - 1)q_\infty/\Gamma_\infty$ ,

$$n_0 = \frac{-\Gamma_\infty \lambda_n}{D(Z_0)}, \quad T_0 = \frac{T_\infty}{1 + \lambda_n/(\lambda_T \zeta)}.$$

The steady state  $\tilde{Z}$  must satisfy (see [4])

$$-\mu \frac{\partial^2 \tilde{Z}}{\partial x^2} = -\frac{T_\infty \Gamma_\infty}{\tilde{n}^2 D(\tilde{Z})} \left( c_n + c_g \left( \frac{\tilde{n}}{n_0} \right)^{-\zeta} \right) + G(\tilde{Z}), \quad (32)$$

where

$$c_g = \frac{\zeta c_T - c_n}{1 + \zeta \lambda_T / \lambda_n}.$$

Using the boundary condition for  $Z$  at  $x = 0$  from (28), it follows that  $Z_0 := \tilde{Z}(x=0)$  is a root of

$$-\frac{T_\infty}{\Gamma_\infty \lambda_n^2} (c_n + c_g) D(Z_0) + G(Z_0) = 0. \quad (33)$$

Next, we consider the situation  $x \rightarrow +\infty$ . It follows now from (30) that  $\tilde{n}(x) \rightarrow +\infty$  (assuming that  $D(Z) > 0$ , which is the only physically meaningful situation). Also, the boundary condition for  $Z$  in (29) gives that  $\partial^2 Z / \partial x^2 \rightarrow 0$  (when  $x \rightarrow +\infty$ ). Substituting these two results into (32) gives

$$G(Z_\infty) = 0, \quad (34)$$

where  $Z_\infty := \lim_{x \rightarrow +\infty} Z(x)$ .

Our observations suggest that there is a unique solution  $\tilde{Z}$  for given  $Z_0$  and  $Z_\infty$ . However, a proof of this statement is missing. It should be noted that (33) and (34) can have multiple roots (typically 3), which means that there will be multiple equilibrium solutions for the same parameter values. Especially the value of  $Z_0$  is of interest, because a higher value of  $Z_0$  reduces the diffusivity at the edge  $D(Z_0)$  (since  $D_1 < 0$ ). This results in the formation of the transport barrier near the edge, which is typical for the H-mode. So by comparing the value of  $Z_0$  of different equilibrium profiles, L-mode and H-mode profiles can be distinguished.

### 3.3. Approximation of equilibrium solutions

In order to find an equilibrium solution from which the continuation can be started, we now derive analytic approximations of the equilibrium solutions. Starting from this analytic approximation, the equilibrium is found by Newton iteration. We focus on constructing an approximate solution  $\tilde{Z}$  of (32);  $\tilde{n}$  and  $\tilde{T}$  are then computed by (30) and (31), respectively.

Recall that (33) typically has multiple roots  $Z_0$ , which means that there will be coexisting equilibrium solutions at one particular set of parameters. Depending on the choice of  $Z_0$ , either an L-mode or an H-mode profile will be constructed. When constructing an L-mode profile, we use  $\tilde{Z} \equiv Z_\infty$ , where  $Z_\infty$  is a root of (34).

To construct an H-mode profile, we approximate  $\tilde{n} \approx n_0$  near the edge  $x = 0$ . Using this in (32) leads to

$$\begin{aligned} -\mu \frac{\partial^2 \tilde{Z}}{\partial x^2} &\approx -\frac{T_\infty \Gamma_\infty}{n_0^2 D(\tilde{Z})} (c_n + c_g) + G(\tilde{Z}) \\ &= \frac{D(Z_0)G(Z_0)}{D(\tilde{Z})} + G(\tilde{Z}). \end{aligned} \quad (35)$$

Here, the last equality follows from (33). Replacing  $1/D(\tilde{Z})$  by its third order Taylor approximation around  $Z = Z_S$ , we obtain an equation of the form

$$\mu \frac{\partial^2 \tilde{Z}}{\partial x^2} \approx c(\tilde{Z} - Z_L)(\tilde{Z} - Z_2)(\tilde{Z} - Z_3). \quad (36)$$

When all three roots are real, we order them so that  $Z_L \leq Z_2 \leq Z_3$  and introduce  $z_2 := Z_2 - Z_L$  and  $z_3 := Z_3 - Z_L$ . Now, we approximate  $\tilde{Z}$  by the solution of (36)

$$\tilde{Z}(x) \approx Z_L + z_3 \frac{q_- + 1}{q_- + e^{kx}} \frac{q_+ + 1}{q_+ + e^{-kx}}, \quad (37)$$

where

$$k = \sqrt{\frac{c}{\mu} z_2 z_3},$$

$$q_\pm = \sqrt{2z_3 - z_2} \frac{\sqrt{2}\sqrt{2z_3 - z_2} \pm \sqrt{3z_3}}{(\sqrt{2z_3} + \sqrt{z_2})(\sqrt{z_3} + \sqrt{2z_2})}.$$

In Fig. 4, the constructed approximations are compared to the equilibrium solutions of an accurate spatial discretization discussed below. For the L-mode,  $Z$  indeed approaches the approximation  $Z \equiv Z_\infty$ . For the H-mode the approximation is accurate near  $x = 0$ , but is less accurate for  $x > 0$ . This is a consequence of the assumption  $\tilde{n} = n_0$ , which is only valid near the edge  $x = 0$ .

### 3.4. Discretization

We use a nonuniform grid on the truncated domain  $[0, L]$

$$\Theta := \{0 = x_0 < x_1 < x_2 < \dots < x_N = L\}. \quad (38)$$

Two discretization methods have been investigated: (1) the standard Finite Difference Method (FDM) and (2) a method based on the Finite Volume Method (FVM). The FVM is considered because (21) and (22) represent physical conservation laws.

Based on the well-known finite difference formulas on a nonuniform grid (see for example [19]), the FDM results in  $3(N-1)$  equations. The FVM-based method uses the following  $3N - 1$  unknowns:

$$\bar{n}_i = \int_{x_{i-1}}^{x_i} n(x') dx', \quad 1 \leq i \leq N, \quad (39)$$

$$\bar{U}_i = \int_{x_{i-1}}^{x_i} U(x') dx', \quad 1 \leq i \leq N, \quad (40)$$

$$Z_i = Z(x_i), \quad 1 \leq i \leq N-1. \quad (41)$$

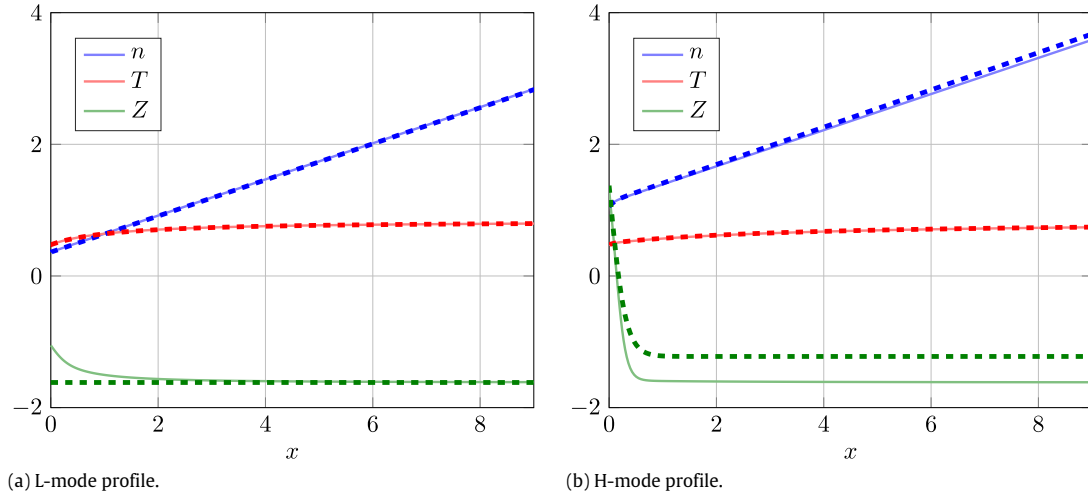


**Fig. 4.** Analytic approximation (dashed) compared to the equilibria of an accurate spatial discretization (solid) at  $b = -2$ .

We use point-wise values for  $Z$ , because (23) does not represent a conservation law. To illustrate this method, we provide an explicit formula

$$\frac{\partial \bar{n}_i}{\partial t} = -\frac{\Gamma_i - \Gamma_{i-1}}{x_i - x_{i-1}}, \quad \Gamma_i := -D(Z_i) \frac{\partial^2 n_i^{tot}}{\partial x^2}, \quad (42)$$

for the discretization of (21). Here, the function  $n^{tot}$  is defined as

$$n^{tot}(x) := \int_0^x n(x') dx', \quad (43)$$

which can be computed in the grid points as

$$n_i^{tot} := n^{tot}(x_i) = \sum_{j=1}^i \bar{n}_j. \quad (44)$$

The derivatives of  $n^{tot}$  are computed by finite differences from  $n_i^{tot}$ .

We observed that the accuracy of both methods is mainly dependent on the distribution of the grid points. For the same grid distribution, the FVM-based method showed a slightly better accuracy. However, the FDM results in a sparser Jacobian matrix  $A$  and was numerically more stable during the continuation. Therefore the FDM was used.

The most accurate results were obtained using Bakhvalov-type meshes [22], namely by accumulating the grid points near the plasma edge  $x = 0$  as

$$x_i = L \left( \frac{i}{N} \right)^m, \quad (45)$$

with  $m = 3$ . The results for  $m = 1$  and  $m = 2$  were less accurate, and choosing  $m = 4$  led to numerical instabilities, due to an extremely small grid spacing near the edge  $x = 0$ .

## 4. Numerical continuation

### 4.1. 1-parameter continuation

The equilibrium solutions of the spatial discretization have been continued in heat flux  $q_\infty$  using CL\_MATCONTL. For  $b$  between  $-2.5$  and  $0$ , we observed four qualitatively different slices. These are shown in Fig. 5. The y-axis in Fig. 5 shows  $Z_0 := Z(x = 0)$ . Recall from Section 3.2 that a low value of  $Z_0$  indicates an L-mode profile and a high value of  $Z_0$  indicates an H-mode profile.

The three types of L–H transitions that have been observed in experiments can be recognized in these slices. In Fig. 5(a) the smooth transitions can be recognized; when the heat flux  $q_\infty$  is increased the profile is smoothly changed from L-mode to H-mode. In Fig. 5(b) the oscillatory transitions can be recognized; between the two Hopf bifurcations there are no stable stationary solutions, which means that oscillations will be observed in the steady-state behavior. In Fig. 5(c) and (d) sharp transitions can be recognized. When starting in L-mode and increasing the heat flux  $q_\infty$ , the equilibrium becomes unstable at the Hopf bifurcation. At this point a sharp transition to the H-mode will be observed. When decreasing the heat flux, starting in an H-mode profile, the transition to L-mode can either occur at the Hopf bifurcation (Fig. 5(c)) or at the LP one (Fig. 5(d)). Note, Fig. 5(c) and (d) indicate the presence of hysteresis.

### 4.2. 2-parameter continuation

In the 2-parameter continuation, the parameters  $b$  and  $q_\infty$  are free. For values of  $a$  between  $-1$  and  $0$ , we observed three qualitatively different slices. These are presented in Fig. 6.

Fig. 6(a) shows the slice at  $a = -1$ . Since this is also the value of  $a$  in Fig. 5, the slices in Fig. 5 can be recognized as lines for  $b = \text{const}$  in Fig. 6(a). Now the arrangement of the three different L–H transitions (that appear when varying the heat flux  $q_\infty$ ) becomes clear from Fig. 6(a): left of the self intersection of the Hopf-curve sharp transitions will be observed, inside the loop in the Hopf curve oscillatory transitions will be observed, and right of the Hopf loop smooth transitions are observed.

The normal form coefficients  $a_2$  and  $b_2$  have been computed at the BT point and satisfy  $a_2 b_2 > 0$ . This indicates that the Hopf bifurcations near the BT point are subcritical (generate an unstable cycle). The Hopf bifurcations become supercritical (generate a stable cycle) at the nearby GH point. To see whether the slice in Fig. 6(a) is near a dBT bifurcation, we compare Fig. 6(a) to the slices Figs. 1, 2, and 3, which show the arrangement of bifurcations expected the three considered dBT bifurcations. The Hopf-curve in Fig. 6(a) and the Hopf-curve in Fig. 3 both show a loop around the CP bifurcation (in Figs. 1 and 2 no such loop can be observed). However, the GH point in Fig. 6(a) is located outside the loop in the H-curve, whereas Fig. 3 shows two GH bifurcations inside the Hopf-loop. This means that the situation in Fig. 6(a) does not indicate a nearby dBT bifurcation.

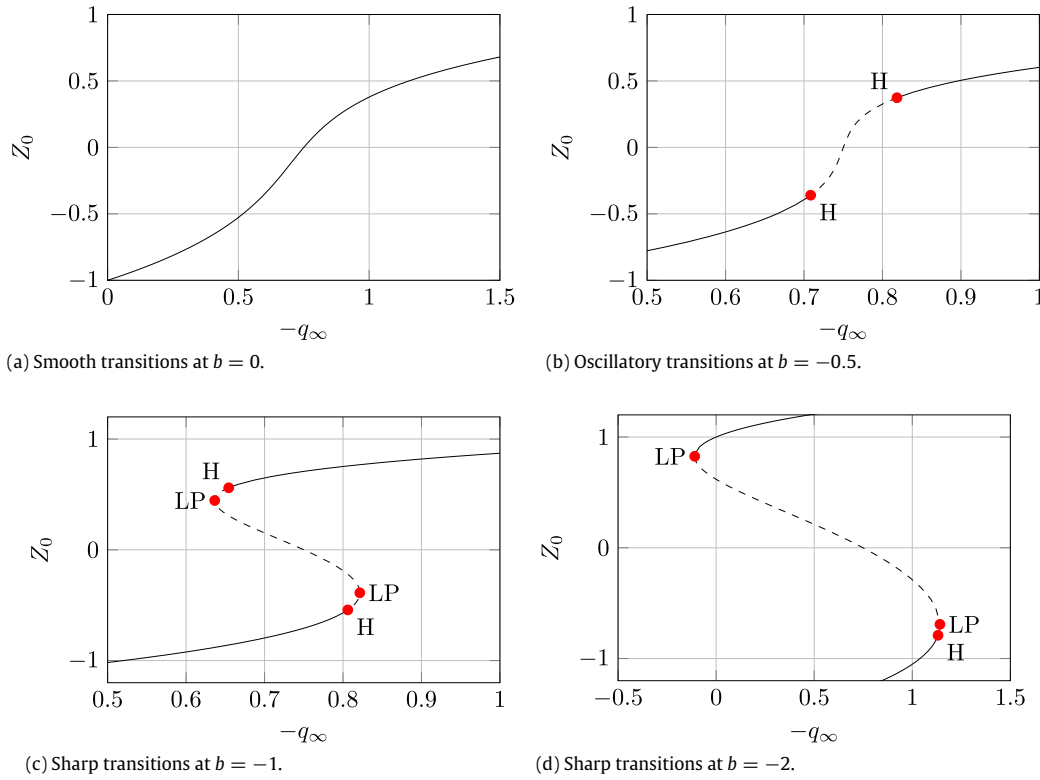


**Fig. 5.** Equilibrium continuation in  $q_\infty$  (solid lines indicate stable profiles and dashed lines indicate unstable profiles).

The slice at  $a = -0.01$  is shown in Fig. 6(b). Now there are two GH bifurcations inside the Hopf-loop, just as in Fig. 3. This change indicates that this slice is closer to the dBT bifurcation. This is also indicated by the global bifurcation curves in Fig. 7 computed in MATCONT, which show the same arrangement as the curves in Fig. 3. Because CL\_MATCONT does not support global bifurcations, the curves in Fig. 7 could only be computed for a relatively low number of grid points  $N = 10$ , whereas the local bifurcation curves in Fig. 6 have been computed for  $N = 50$  grid points. It should also be noted that the curve labeled ‘Hom’ in Fig. 7 was computed as a curve of cycles with large period, which means that HHS and HSN curves could not be distinguished. This also explains why the LP and Hom curves do not precisely overlap at the HSN curve.

All three types of L–H transitions can be recognized in the slice in Figs. 6(b) and 7(a): left of the LPC curve sharp transitions will be observed, inside the region bounded by the LPC and H curves oscillatory transitions will be observed, and right of the Hopf loop smooth transitions are observed. Note however that bifurcation scenario inside the Hopf-loop of Fig. 6(a) is different from the one in the slice of Fig. 6(b) and that the scenario in Fig. 6(b) was the one expected in [4].

The slice at  $a = -0.005$  is shown in Fig. 6(c). The BT point has moved to the other side of the CP point. This suggests that for some value of  $a$  between  $-0.01$  and  $-0.005$  the BT switches branches passing through the CP point, indicating a degenerate BT bifurcation. In the slice in Fig. 6(c) only sharp and smooth transitions can be recognized, and oscillatory transitions are absent: left of the CP point sharp transitions will be observed and right of the CP point smooth transitions are observed.

#### 4.3. 3-parameter continuation

To confirm that the dBT occurs between  $a = -0.01$  and  $a = -0.005$  and to determine the type of the degeneracy, the BT point

in Fig. 6(b) is continued in the parameters  $q_\infty$ ,  $b$  and  $a$ . The resulting curve is shown in Fig. 8. Along this curve the normal form coefficients  $a_2$  and  $b_2$  are computed. In the point labeled ‘dBT’ both coefficients vanish simultaneously (up to numerical inaccuracies). This indicates that near this point the restriction of the system to the center manifold is topologically equivalent to a system induced from the system (6), by a (possibly noninvertible) parameter transformation. Using the formulas in [15], the normal form coefficients  $a_3$  and  $b_3$  could be computed in this point. Both coefficients are nonzero and  $a_3 < 0$ , indicating that the bifurcation diagram in Fig. 3 and the results in [18] indeed apply for this situation. This is consistent with the codimension-2 slices in Figs. 6(b), 7, and 6(c), which show a good correspondence to the slice in the system (6) in Fig. 3 and the results in [18].

As was already observed in [4], the presence of this codimension-4 bifurcation indicates the presence of all three L–H transitions nearby. However, the arrangement of the different transition regimes cannot be determined based on the 3-parameter continuation, but should be found by computing nearby 2-parameter slices as in Figs. 6 and 7.

## 5. Discussion

The simultaneous vanishing of both normal form coefficients is a codimension-4 degeneracy, which is generically not found in 3-parameter families. This could indicate that the choice of parameters in Table 3 is nongeneric. This hypothesis was tested by varying all 15 parameters in Table 3 independently (by approximately 30% of their value). In all situations, simultaneous vanishing of both normal form coefficients was observed (up to numerical inaccuracies). This indicates that the simultaneous vanishing of both coefficients is not caused by a nongeneric choice of parameter values in Table 3.



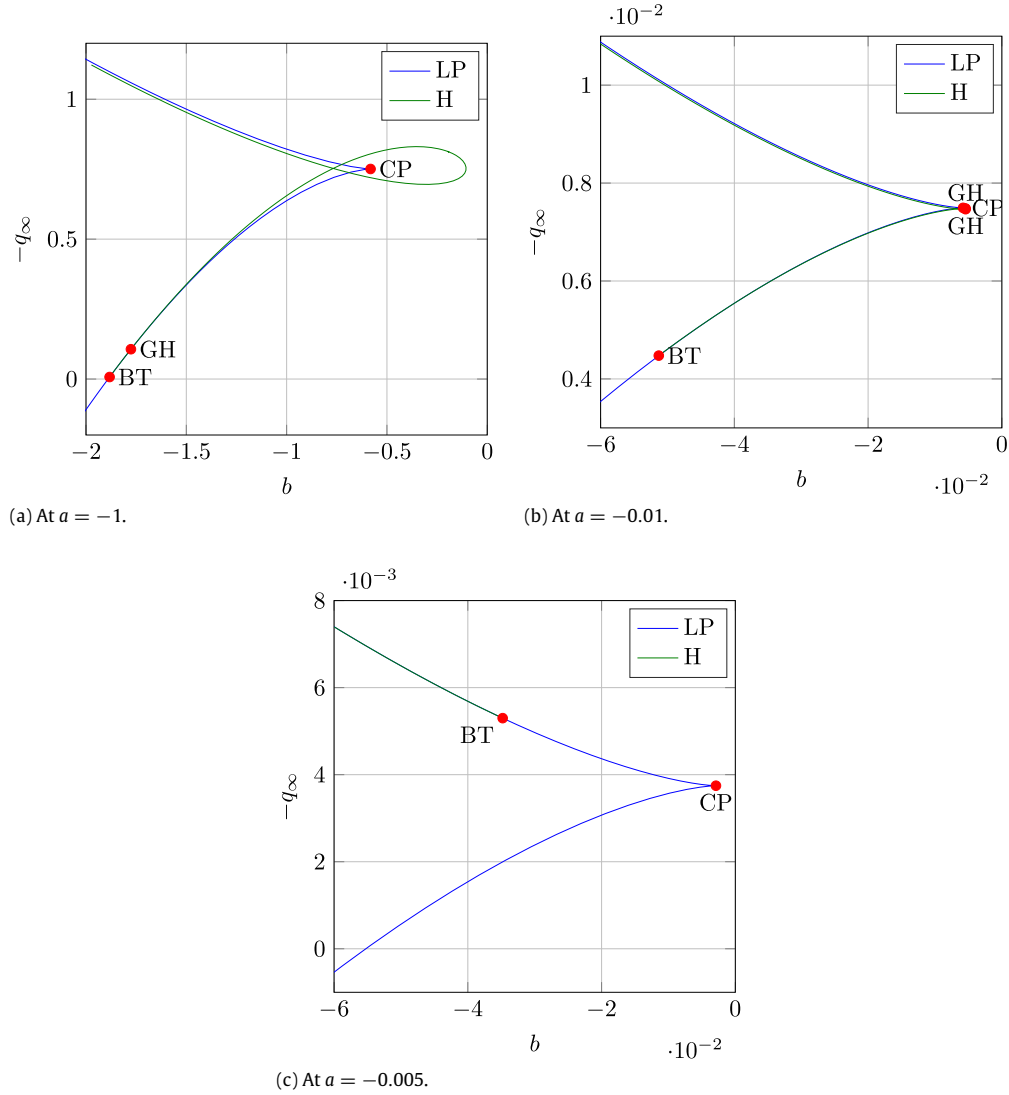


**Fig. 6.** Two parameter continuation in  $b$  and  $q_\infty$ .

We have also investigated whether the simultaneous vanishing is caused by some (over)simplifications in the model. The following alternative parametrizations of the diffusion  $D(Z)$  and the conductivity  $\chi(Z)$  have been considered,

$$D(Z) = D_0 + D_1 \tanh(Z) + D_2 \tanh^2(Z), \quad (46)$$

$$\chi(Z) = \frac{1}{(\gamma - 1)\zeta} D(Z + Z_S^*). \quad (47)$$

Note that the original  $D(Z)$  and  $\chi(Z)$  in (24) and (25) appear for  $D_2 = Z_S^* = 0$ . Also the boundary condition for  $Z$  in (28) was modified to a Robin boundary condition

$$\frac{\partial Z}{\partial x} = \frac{Z}{\lambda_Z}. \quad (48)$$

Also under these modifications, simultaneous vanishing of both normal form coefficients was observed.

A closer inspection of the components of  $b_2$  in (20) shows that  $p_0^\top f_{uu}[q_0, q_0]$  and  $p_1^\top f_{uu}[q_0, q_1]$  also vanish (apparently) simultaneously at the dBT. This is an additional indication that the quadratic terms at the dBT are nongeneric. Whether or not this phenomena is related to the transport nature of Eqs. (21)–(23) remains unclear.

In the generic unfolding of the codimension-4 dBT bifurcation (6), there are parameter values  $\beta$  near  $\beta = 0$  for which one of the normal form coefficients of the BT bifurcation vanishes while the other one is nonzero. In the considered transport model this situation could not be observed, which means that the located dBT bifurcation does not completely unfold in the considered parameters, i.e. we only see a 3-dimensional hypersurface in the 4-dimensional parameter space of (6).

It should also be noted that the presence of the dBT bifurcation only provides information about the *local* bifurcation scenario, and that not all of the dynamics in (21)–(23) resembles the one near a dBT bifurcation. This is also illustrated by the slice in Fig. 6(a), in which the location of the GH bifurcation points is not the same as near a dBT of codimension 4. In a (limited) study of the global bifurcations in the slice at  $a = -1$  for  $N = 10$  grid points, we observed period doubling and saddle-focus homoclinic orbits, which indicates a much more complex bifurcation scenario. The observed limit cycle near a saddle-focus homoclinic bifurcation can also be found for  $N = 50$  grid points and is shown in Fig. 9.

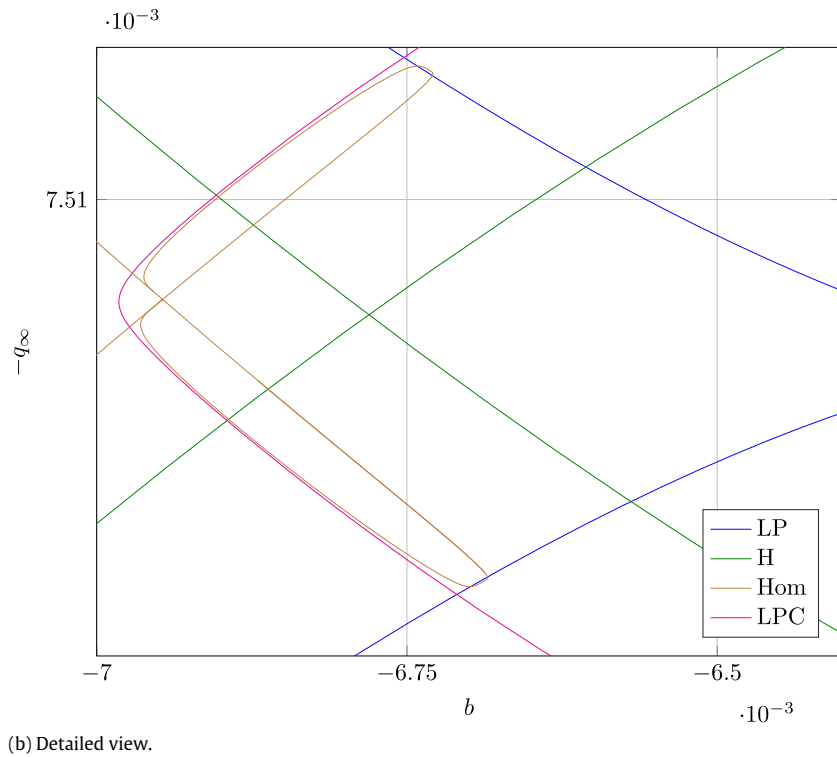
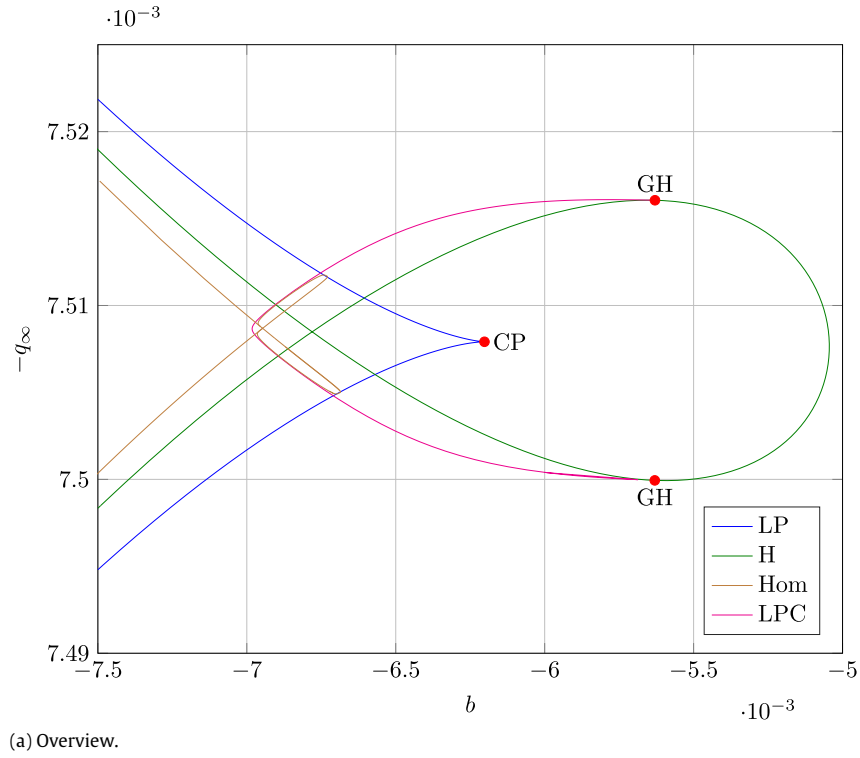


**Fig. 7.** Global bifurcation curves at  $a = -0.01$  computed in MATCONT.

The accuracy of the used spatial discretization is illustrated by Fig. 10, which shows the Hopf and LP curves in Fig. 6(a) for  $N = 15$ ,  $N = 30$  and  $N = 50$  grid points. The curves for  $N = 30$  and  $N = 50$  overlap almost completely, indicating that the results for  $N = 50$  are accurate. In the same way, the convergence of the spatial discretization has been established for all results in

Figs. 5, 6, and 8. For the curves in Fig. 7 this was not possible due to excessive computation times.

#### Acknowledgments

This project was carried out with financial support from NWO. The work has been carried out within the framework of the EU-

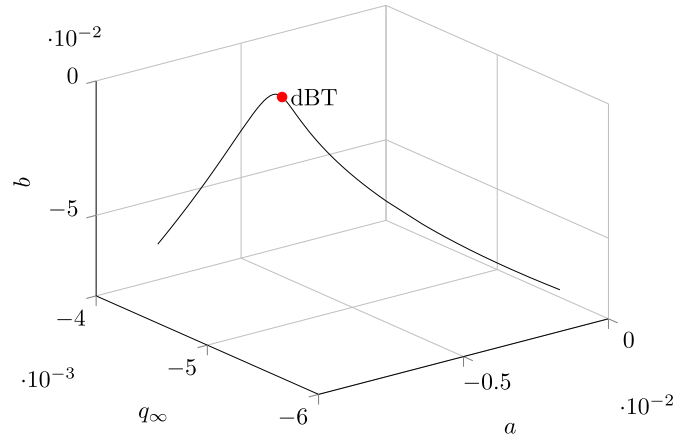


**Fig. 8.** The degenerate BT bifurcation (dBT) on the curve of BT bifurcations.

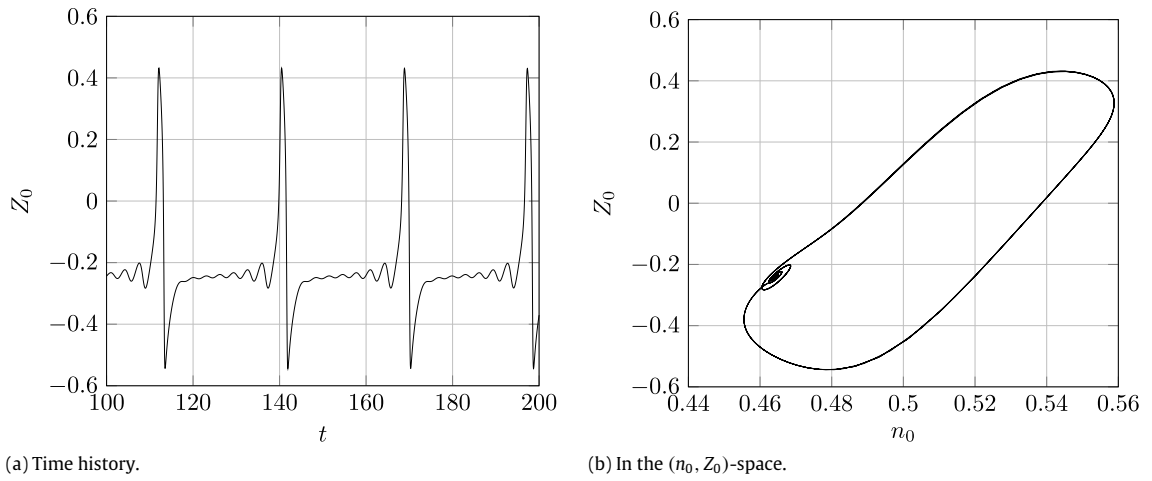


**Fig. 9.** Periodic orbit near a saddle-focus homoclinic orbit (at  $q_\infty = -0.7$ ,  $b = -0.3$ , and  $a = -1$  for  $N = 50$  grid points).

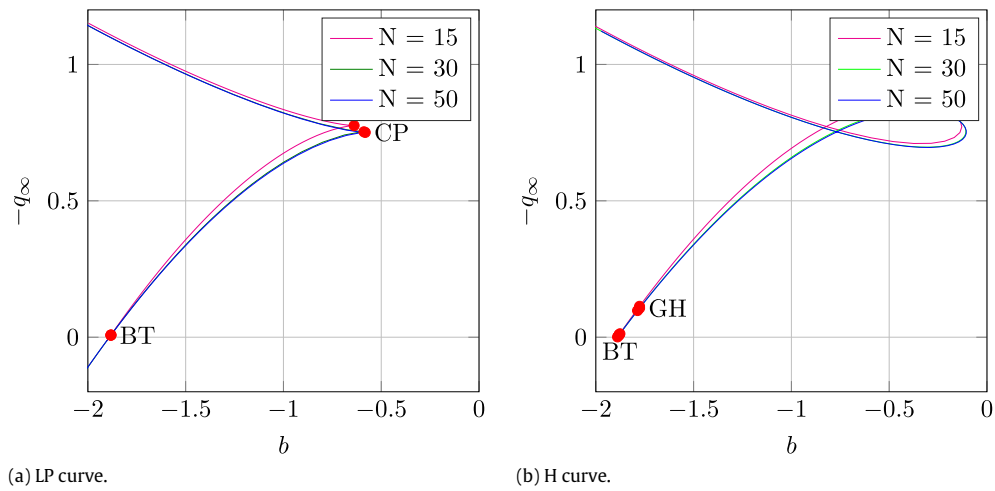


**Fig. 10.** Convergence of the H and LP curves at  $a = -1$  in Fig. 6(a).

ROfusion Consortium and has received funding from the Euratom research and training programme 2014–2018 under Grant Agreement No. 633053. The views and opinions expressed herein do not necessarily reflect those of the European Commission.

## Appendix. Implementation in `cl_matcontL`

### A.1. Detection of Hopf bifurcations

Compared to the detection of Hopf-bifurcations in [7], the second test function  $\psi_H^{(2)}$  was changed to

$$\psi_H^{(2)} = m_u$$

where  $m_u$  equals the number of unstable eigenvalues of the restriction  $C$  in (10). We now only check for a Hopf bifurcation (using  $\psi_H^{(1)}$  from [7]) when the value of  $\psi_H^{(2)}$  changes. This implementation is more robust in situations where a Hopf and a neutral saddle are close to each other.

### A.2. The Hopf curve

The defining system for the Hopf curve is  $F(X) = 0$ , where

$$X = (u, \alpha, \kappa) \in \mathbb{R}^n \times \mathbb{R}^2 \times \mathbb{R}, \quad F(X) = \begin{pmatrix} f(u, \alpha) \\ g_{i_1 j_1}(u, \alpha, \kappa) \\ g_{i_2 j_2}(u, \alpha, \kappa) \end{pmatrix},$$

where the  $g_{ij}$ ,  $i, j \in \{1, 2\}$  are computed as in [7] via

$$\begin{bmatrix} C^2 + \kappa I_m & \hat{w}_{1, \text{bor}} & \hat{w}_{2, \text{bor}} \\ \hat{v}_{1, \text{bor}}^\top & 0 & 0 \\ \hat{v}_{2, \text{bor}}^\top & 0 & 0 \end{bmatrix} \begin{bmatrix} \hat{v}_1 & \hat{v}_2 \\ g_{11} & g_{12} \\ g_{21} & g_{22} \end{bmatrix} = \begin{bmatrix} 0_m & 0_m \\ 1 & 0 \\ 0 & 1 \end{bmatrix}. \quad (\text{A.1})$$

The borders  $\hat{v}_{1, \text{bor}}, \hat{v}_{2, \text{bor}}, \hat{w}_{1, \text{bor}}, \hat{w}_{2, \text{bor}} \in \mathbb{R}^m$  are selected such that the matrix on the left of (A.1) is non-singular and the coefficients  $i_1, j_1, i_2$  and  $j_2$  are selected as in [7]. The Jacobian matrix now becomes

$$F_X = \begin{bmatrix} A & f_\alpha & 0_n \\ g_{i_1 j_1, u} & g_{i_1 j_1, \alpha} & g_{i_1 j_1, \kappa} \\ g_{i_2 j_2, u} & g_{i_2 j_2, \alpha} & g_{i_2 j_2, \kappa} \end{bmatrix}. \quad (\text{A.2})$$

The derivatives of  $g_{i_1 j_1}$  and  $g_{i_2 j_2}$  are computed differently from those in [7]. Their computation is based on an application of the following lemma with  $M = A^2 + \kappa I$ .

**Lemma 2.** Let  $M = M(X) \in \mathbb{R}^{n \times n}$ ,  $Q = Q(X) \in \mathbb{R}^{n \times m}$  and assume that the columns of  $Q$  span an invariant subspace of  $M$ . Define  $G \in \mathbb{R}^{k \times k}$  as the solution of

$$\begin{bmatrix} Q^\top M Q & \hat{w}_{\text{bor}} \\ \hat{v}_{\text{bor}}^\top & 0_{k \times k} \end{bmatrix} \begin{bmatrix} \hat{v} \\ G \end{bmatrix} = \begin{bmatrix} 0_{m \times k} \\ I_k \end{bmatrix}, \quad (\text{A.3})$$

where  $I_k$  denotes the  $(k \times k)$ -identity matrix. Assume that the borders  $\hat{v}_{\text{bor}}, \hat{w}_{\text{bor}} \in \mathbb{R}^{m \times k}$  are selected such that the matrix on the left of (A.3) is nonsingular. Now introduce  $W$  by

$$\begin{bmatrix} M^\top & Q \hat{v}_{\text{bor}} \\ \hat{w}_{\text{bor}}^\top Q_1^\top & 0_{k \times k} \end{bmatrix} \begin{bmatrix} W \\ \tilde{G} \end{bmatrix} = \begin{bmatrix} 0_{n \times k} \\ I_k \end{bmatrix}. \quad (\text{A.4})$$

Then the matrix on the left of (A.4) is also non-singular,  $G = \tilde{G}^\top$ , and at a point  $X_0$  for which  $G(X_0) = 0_{k \times k}$  it holds that

$$G_X(X_0) = -\hat{W} M_X Q_1 \hat{v}. \quad (\text{A.5})$$

**Proof.** For a contradiction, assume that the matrix on the left of (A.4) is singular. Then its transpose has a nonzero null vector, i.e. there exist  $V_0 \in \mathbb{R}^n$  and  $G_0 \in \mathbb{R}^k$  such that

$$\begin{bmatrix} M & Q \hat{w}_{\text{bor}} \\ \hat{v}_{\text{bor}}^\top Q^\top & 0_{k \times k} \end{bmatrix} \begin{bmatrix} V_0 \\ G_0 \end{bmatrix} = \begin{bmatrix} 0_{n \times k} \\ 0_{k \times k} \end{bmatrix}.$$

Hence  $MV_0 = -Q \hat{w}_{\text{bor}} G_0$  is in the range of  $Q$ . Since the columns of  $Q$  span an invariant subspace of  $M$ , it follows that there exists a  $\hat{v}_0 \in \mathbb{R}^m$  s.t.  $MV_0 = MQ_1 \hat{v}_0$ . Now

$$\begin{bmatrix} Q_1^\top M Q_1 & \hat{w}_{\text{bor}} \\ \hat{v}_{\text{bor}}^\top & 0_{k \times k} \end{bmatrix} \begin{bmatrix} \hat{v}_0 \\ G_0 \end{bmatrix} = \begin{bmatrix} 0_{m \times k} \\ 0_{k \times k} \end{bmatrix}.$$

This contradicts the assumption that the matrix on the left of (A.3) is non-singular.

Now denote  $V := Q \hat{v}$ . Now (A.3) implies

$$\underbrace{\begin{bmatrix} M & Q_1 \hat{w}_{\text{bor}} \\ \hat{v}_{\text{bor}}^\top Q_1^\top & 0_k \end{bmatrix}}_{=: N} \begin{bmatrix} V \\ G \end{bmatrix} = \begin{bmatrix} 0_{n \times k} \\ I_k \end{bmatrix}. \quad (\text{A.6})$$

We introduce  $N$  as the matrix on the left of (A.6). Note that the matrix on the left of (A.4) is  $N^\top$ . Now (A.6) and (A.4) imply that

$$G = [0_{k \times n} \quad I_k] N^{-1} \begin{bmatrix} 0_{n \times k} \\ I_k \end{bmatrix},$$

$$\tilde{G} = [0_{k \times n} \quad I_k] N^{-\top} \begin{bmatrix} 0_{n \times k} \\ I_k \end{bmatrix},$$

which gives  $G = \tilde{G}^\top$ .

Differentiating the first line of (A.6) w.r.t.  $X$  and rearranging the terms lead to

$$Q_1 \hat{w}_{\text{bor}} G_X = -M_X V - M V_X - Q_{1X} \hat{w}_{\text{bor}} G. \quad (\text{A.7})$$

The last term in (A.7) vanishes because  $G(X_0) = 0_{k \times k}$ . Multiplying Eq. (A.7) from the right by  $W^\top$  gives

$$G_X = -W^\top M_X V - W^\top M V_X. \quad (\text{A.8})$$

Here it was used that (A.4) with  $\tilde{G} = G^\top = 0_{k \times k}$  shows that  $\hat{w}_{\text{bor}}^\top Q_1^\top W = I_k$ . Eq. (A.4) also implies that  $M^\top W = 0_{n \times k}$  for  $G = 0_{k \times k}$ , so that the result follows.  $\square$

Based on this result, we compute the derivatives of  $g_{ij}$  by

$$g_{ij, u} = -W_i^\top (A A_u + A_u A) Q \hat{v}_j, \quad (\text{A.9})$$

$$g_{ij, \alpha} = -W_i^\top (A A_\alpha + A_\alpha A) Q \hat{v}_j, \quad (\text{A.10})$$

$$g_{ij, \kappa} = -W_i^\top Q \hat{v}_j, \quad (\text{A.11})$$

where  $\hat{v}_j$  are computed from (A.1) and  $W_i$  are computed by solving

$$\begin{bmatrix} (A^2 + \kappa I_n)^\top & Q \hat{v}_{1, \text{bor}} & Q \hat{v}_{2, \text{bor}} \\ \hat{w}_{1, \text{bor}}^\top Q^\top & 0 & 0 \\ \hat{w}_{2, \text{bor}}^\top Q^\top & 0 & 0 \end{bmatrix} \begin{bmatrix} W_1 & W_2 \\ g_{11} & g_{21} \\ g_{12} & g_{22} \end{bmatrix} = \begin{bmatrix} 0_n & 0_n \\ 1 & 0 \\ 0 & 1 \end{bmatrix}.$$

### A.3. The LP curve

The defining system for the LP curve is  $F(X) = 0$ , with

$$X = (u, \alpha) \in \mathbb{R}^n \times \mathbb{R}^2, \quad F(X) = \begin{pmatrix} f(u, \alpha) \\ g(u, \alpha) \end{pmatrix} \quad (\text{A.12})$$

where  $g$  is computed as the solution to

$$\begin{bmatrix} C & \hat{w}_{\text{bor}} \\ \hat{v}_{\text{bor}}^\top & 0 \end{bmatrix} \begin{bmatrix} v \\ g \end{bmatrix} = \begin{bmatrix} 0_m \\ 1 \end{bmatrix}. \quad (\text{A.13})$$

The borders must be selected such that the matrix on the left of (A.13) is nonsingular. The Jacobian matrix is

$$F_X = \begin{bmatrix} A & f_\alpha \\ g_u & g_\alpha \end{bmatrix}, \quad (\text{A.14})$$

where  $g_u$  and  $g_\alpha$  are computed differently from [7], namely, their computation is based on an application of Lemma 2 with  $M = A$  as

$$g_u = -W^\top A_u Q \hat{v}, \quad g_\alpha = -W^\top A_\alpha Q \hat{v}, \quad (\text{A.15})$$

where  $W$  is computed by solving

$$\begin{bmatrix} A^\top & Q \hat{v}_{\text{bor}} \\ \hat{w}_{\text{bor}}^\top Q^\top & 0 \end{bmatrix} \begin{bmatrix} W \\ g \end{bmatrix} = \begin{bmatrix} 0_n \\ 1 \end{bmatrix}. \quad (\text{A.16})$$

#### A.4. Proof of Lemma 1

**Proof.** Note that (11) is of the form of (A.3) and that (15) is of the form (A.4). Therefore, Lemma 2 (with  $M = A$ ) gives that the matrix on the left of (15) and (16) is nonsingular and that  $g_1 = \tilde{g}_1$ .

Introduce  $V_1 := Q \hat{v}_1$  and  $V_2 := Q \hat{v}_2$  and observe that

$$\begin{bmatrix} M & Q \hat{w}_{\text{bor}} \\ \hat{v}_{\text{bor}}^\top Q^\top & 0 \end{bmatrix} \begin{bmatrix} V_1 \\ g_1 \end{bmatrix} = \begin{bmatrix} 0_n \\ 1 \end{bmatrix}, \quad (\text{A.17})$$

$$\underbrace{\begin{bmatrix} M & Q \hat{w}_{\text{bor}} \\ \hat{v}_{\text{bor}}^\top Q^\top & 0 \end{bmatrix}}_{=:N} \begin{bmatrix} V_2 \\ g_2 \end{bmatrix} = \begin{bmatrix} V_1 \\ 0 \end{bmatrix}. \quad (\text{A.18})$$

To see that  $g_2 = \tilde{g}_2$ , observe that (A.17) and (15) imply

$$\begin{bmatrix} V_1 \\ 0 \end{bmatrix} = N^{-1} \begin{bmatrix} 0_n \\ 1 \end{bmatrix} - g_1 \begin{bmatrix} 0_n \\ 1 \end{bmatrix}, \quad (\text{A.19})$$

$$\begin{bmatrix} W_1 \\ 0 \end{bmatrix} = N^{-\top} \begin{bmatrix} 0_n \\ 1 \end{bmatrix} - g_1 \begin{bmatrix} 0_n \\ 1 \end{bmatrix}. \quad (\text{A.20})$$

Now (A.18) and (A.19) give

$$\begin{aligned} g_2 &= \begin{bmatrix} 0_n^\top & 1 \end{bmatrix} N^{-1} \begin{bmatrix} V_1 \\ 0 \end{bmatrix} \\ &= \begin{bmatrix} 0_n^\top & 1 \end{bmatrix} N^{-2} \begin{bmatrix} 0_n \\ 1 \end{bmatrix} - g_1 \begin{bmatrix} 0_n^\top & 1 \end{bmatrix} N^{-1} \begin{bmatrix} 0_n \\ 1 \end{bmatrix}, \end{aligned}$$

and (16) and (A.20) give

$$\begin{aligned} \tilde{g}_2 &= \begin{bmatrix} 0_n^\top & 1 \end{bmatrix} N^{-\top} \begin{bmatrix} W_1 \\ 0 \end{bmatrix} \\ &= \begin{bmatrix} 0_n^\top & 1 \end{bmatrix} N^{-2\top} \begin{bmatrix} 0_n \\ 1 \end{bmatrix} - g_1 \begin{bmatrix} 0_n^\top & 1 \end{bmatrix} N^{-\top} \begin{bmatrix} 0_n \\ 1 \end{bmatrix}. \end{aligned}$$

These two equations imply that  $g_2 = \tilde{g}_2^\top = \tilde{g}_2$ .

Eq. (17) follows again from Lemma 2. For (18), note that (16) gives

$$A^\top W_2 + Q \hat{v}_{\text{bor}} g_2 = W_1.$$

Taking the transpose and differentiating w.r.t.  $X$  gives

$$W_2^\top A_X + W_{2X}^\top A + g_2^\top \hat{v}_{\text{bor}}^\top Q_X^\top + g_{2X}^\top \hat{v}_{\text{bor}}^\top Q^\top = W_{1X}^\top. \quad (\text{A.21})$$

Multiplying from the right with  $V_1$  results in:

$$W_2^\top A_X V_1 + g_{2X}^\top = W_{1X}^\top V_1. \quad (\text{A.22})$$

Here, the second term vanishes because  $AV_1 = 0_n$  when  $g_1 = 0$  (see (A.17)), the third term vanishes because  $g_2 = 0$ , and the fourth term gives  $g_{2X}$  because  $\hat{v}_{\text{bor}}^\top Q^\top V_1 = 1$  (see also (A.17)).

Now (15) gives that  $A^\top W_1 + Q \hat{v}_{\text{bor}} g_1 = 0_n$ . Taking the transpose and differentiating w.r.t.  $X$  results in

$$W_{1X}^\top A + W_1^\top A_X + g_{1X}^\top \hat{v}_{\text{bor}}^\top Q^\top + g_1^\top \hat{v}_{\text{bor}}^\top Q_X^\top = 0.$$

Multiplying the above from the right by  $V_2$  gives

$$W_{1X}^\top AV_2 + W_1^\top A_X V_2 = 0, \quad (\text{A.23})$$

where the third term vanishes because  $\hat{v}_{\text{bor}}^\top Q^\top V_2 = 0$  and the fourth term vanishes because  $g_1 = 0$ . For  $g_2 = 0$ , (A.18) gives that  $V_1 = AV_2$ , so that

$$W_{1X}^\top V_1 = W_{1X}^\top AV_2. \quad (\text{A.24})$$

Now (A.22) can be rewritten as

$$W_2^\top A_X V_1 + g_{2X}^\top = W_{1X}^\top V_1 \quad (\text{A.25})$$

$$= W_{1X}^\top AV_2 \quad (\text{A.26})$$

$$= -W_1^\top A_X V_2, \quad (\text{A.27})$$

where the second equality follows from (A.24), and the third equality follows from (A.23). This is precisely (18).  $\square$

## References

- [1] F. Wagner, et al., Regime of improved confinement and high beta in neutral-beam-heated divertor discharges of the ASDEX tokamak, Phys. Rev. Lett. 49 (1982) 1408–1412. URL: <http://link.aps.org/doi/10.1103/PhysRevLett.49.1408>.
- [2] S.-I. Itoh, K. Itoh, A. Fukuyama, Y. Miura, Edge localized mode activity as a limit cycle in tokamak plasmas, Phys. Rev. Lett. 67 (1991) 2485–2488. URL: <http://link.aps.org/doi/10.1103/PhysRevLett.67.2485>.
- [3] H. Zohm, Dynamic behavior of the L–H transition, Phys. Rev. Lett. 72 (1994) 222–225. URL: <http://link.aps.org/doi/10.1103/PhysRevLett.72.222>.
- [4] W. Weymies, H.J. de Blank, G.M.D. Hogewei, J.C. de Valena, Bifurcation theory for the L–H transition in magnetically confined fusion plasmas, Phys. Plasmas 19 (7) (2012) 1063. URL: <http://scitation.aip.org/content/aip/journal/pop/19/7/10.1063/1.4739227>.
- [5] W. Weymies, H.J. de Blank, G.M.D. Hogewei, Bifurcation theory of a one-dimensional transport model for the L–H transition, Phys. Plasmas 20 (8) (2013) 4817945. URL: <http://scitation.aip.org/content/aip/journal/pop/20/8/10.1063/1.4817945>.
- [6] W. Weymies, S. Paquay, H.J. de Blank, G.M.D. Hogewei, Comparison of bifurcation dynamics of turbulent transport models for the L–H transition, Phys. Plasmas 21 (5) (2014) 5. URL: <http://scitation.aip.org/content/aip/journal/pop/21/5/10.1063/1.4871856>.
- [7] D. Bindel, M. Friedman, W. Govaerts, J. Hughes, Yu.A. Kuznetsov, Numerical computation of bifurcations in large equilibrium systems in MATLAB, J. Comput. Appl. Math. 261 (2014) 232–248. URL: <http://dx.doi.org/10.1016/j.cam.2013.10.034>.
- [8] D. Bindel, W. Govaerts, J. Hughes, Yu.A. Kuznetsov, M. Pekkér, D. Veldman, CL\_MATCONT: continuation toolbox in matlab, Oct. 2015. URL: <http://uuh.edu/faculty/pekker>.
- [9] D. Bindel, J. Demmel, M. Friedman, Continuation of invariant subspaces in large bifurcation problems, SIAM J. Sci. Comput. 30 (2) (2008) 637–656. URL: <http://dx.doi.org/10.1137/060654219>.
- [10] A. Dhooge, W. Govaerts, Yu.A. Kuznetsov, W. Mestrom, A. Riet, B. Sautois, MATCONT and CL\_MATCONT: Continuation Toolboxes in Matlab, Universiteit Gent, Belgium and Utrecht University, The Netherlands, 2006, URL: <http://sourceforge.net/projects/matcont>.
- [11] V. De Witte, W. Govaerts, Yu.A. Kuznetsov, M. Friedman, Interactive initialization and continuation of homoclinic and heteroclinic orbits in MATLAB, ACM Trans. Math. Software 38 (3) (2012) 34. URL: <http://dx.doi.org/10.1145/2168773.2168776>.
- [12] A. Dhooge, W. Govaerts, Yu.A. Kuznetsov, H.G.E. Meijer, B. Sautois, New features of the software MatCont for bifurcation analysis of dynamical systems, Math. Comput. Model. Dyn. Syst. 14 (2) (2008) 147–175. URL: <http://dx.doi.org/10.1080/13873950701742754>.
- [13] Yu.A. Kuznetsov, Elements of Applied Bifurcation Theory, third ed., in: Applied Mathematical Sciences, vol. 112, Springer-Verlag, New York, 2004.
- [14] V.I. Arnol'd, Geometrical Methods in the Theory of Ordinary Differential Equations, second ed., in: Grundlehren der Mathematischen Wissenschaften (Fundamental Principles of Mathematical Sciences), vol. 250, Springer-Verlag, New York, 1988, translated from the Russian by Joseph Szűcs [József M. Szűcs].
- [15] Yu.A. Kuznetsov, Practical computation of normal forms on center manifolds at degenerate Bogdanov–Takens bifurcations, Internat. J. Bifur. Chaos Appl. Sci. Engrg. 15 (11) (2005) 3535–3546. URL: <http://dx.doi.org/10.1142/S0218127405014209>.



- [16] F. Dumortier, R. Roussarie, J. Sotomayor, Generic 3-parameter families of vector fields on the plane, unfolding a singularity with nilpotent linear part. The cusp case of codimension 3, *Ergodic Theory Dynam. Systems* 7 (3) (1987) 375–413. URL: <http://dx.doi.org/10.1017/S0143385700004119>.
- [17] F. Dumortier, R. Roussarie, J. Sotomayor, H. Żoładek, *Bifurcations of Planar Vector Fields: Nilpotent Singularities and Abelian Integrals*, in: *Lecture Notes in Mathematics*, vol. 1480, Springer-Verlag, Berlin, 1991.
- [18] A.I. Khibnik, B. Krauskopf, C. Rousseau, Global study of a family of cubic Liénard equations, *Nonlinearity* 11 (6) (1998) 1505–1519. URL: <http://dx.doi.org/10.1088/0951-7715/11/6/005>.
- [19] W.J.F. Govaerts, *Numerical Methods for Bifurcations of Dynamical Equilibria*, Society for Industrial and Applied Mathematics (SIAM), Philadelphia, PA, 2000, URL: <http://dx.doi.org/10.1137/1.9780898719543>.
- [20] W.-J. Beyn, A. Champneys, E. Doedel, W. Govaerts, Yu.A. Kuznetsov, B. Sandstede, Numerical continuation, and computation of normal forms, in: *Handbook of Dynamical Systems*, Vol. 2, Elsevier, 2002, pp. 149–219. URL: [http://dx.doi.org/10.1016/S1874-575X\(02\)80025-X](http://dx.doi.org/10.1016/S1874-575X(02)80025-X).
- [21] W. Govaerts, Yu.A. Kuznetsov, B. Sijnave, Continuation of codimension-2 equilibrium bifurcations in CONTENT, in: *Numerical Methods for Bifurcation Problems and Large-Scale Dynamical Systems* (Minneapolis, MN, 1997), in: *IMA Vol. Math. Appl.*, vol. 119, Springer, New York, 2000, pp. 163–184. URL: [http://dx.doi.org/10.1007/978-1-4612-1208-9\\_7](http://dx.doi.org/10.1007/978-1-4612-1208-9_7).
- [22] N. Bakhvalov, The optimization of methods of solving boundary value problems with a boundary layer, *USSR Comput. Math. Math. Phys.* 9 (1969) 139–166.